MINIREVIEW

Check for updates

Cu-based bimetallic catalysts for electrochemical CO_2 reduction: before and beyond the tandem effect

Dimiao Luo,[a] Weidong Dai,[a] Keying Wu,[a] Siyuan Liu,[a] Chiyao Tang,[b] Yanjuan Sun,[b] Fan Dong[a] and Chang Long [iD] *[a]

Electrochemical CO_2 reduction reaction (CO_2RR) is a promising approach for carbon reduction and the production of high-value chemicals. Among the various catalysts, Cu-based bimetallic catalysts have recently attracted significant attention due to their superior catalytic activity, often outperforming pure Cu counterparts, owing to the discovery of the tandem effect. This review provides an in-depth discussion of the development of Cu-based bimetallic catalysts for CO_2RR over the past decades, with the discovery, understanding, and evolution of the tandem effect serving as the central thematic thread. Important mile-stone works have been reviewed and organized in a roughly historical manner to highlight the development of cutting-edge understanding and the remaining challenges in this field. We believe this review will help the research community clearly track the progress from the original to the latest findings and identify key insights for Cu-based bimetallic catalysts for CO_2RR.

[a]*Research Center for Carbon-Neutral Environmental & Energy Technology, Institute of Fundamental and Frontier Sciences, University of Electronic Science and Technology of China, Chengdu 611731, Sichuan, P. R. China.*
E-mail: longch@uestc.edu.cn
[b]*School of Resources and Environment, University of Electronic Science and Technology of China, Chengdu 611731, Sichuan, P. R. China*

Chang Long

Chang Long is currently an associate professor at the Institute of Fundamental and Frontier Sciences, University of Electronic Science and Technology of China (UESTC). He earned his BS (2015) and PhD (2021) in materials chemistry from Harbin Institute of Technology under the guidance of Prof. Zhiyong Tang and Prof. Shaoqin Liu. During his PhD, he was a joint student at the National Center for Nanoscience and Technology, Beijing. From 2021 to 2023, he conducted post-doctoral research with Prof. Chunhua Cui and Prof. Fan Dong at UESTC. His research focuses on nanomaterial interfaces and electrochemical applications.

1. Introduction

Excessive anthropogenic emissions of carbon dioxide (CO_2) have severely disrupted the Earth's intrinsic carbon cycle, exacerbating global climate change and posing a significant threat to the sustainability of ecosystems and human society.[1–4] Fortunately, electrochemical CO_2 reduction (CO_2RR) shows great promise in addressing this problem by leveraging renewable electricity to convert CO_2 into chemical feedstocks, such as ethylene, ethanol, and *n*-propanol.[5,6] Moreover, recent techno-economic analyses highlighted the foreseeable economic margins, leading to further increased research attention in CO_2RR.[7–13]

Over the past decades, significant progress has been made in the selective synthesis of mono-carbon (C_1) products in CO_2RR, such as CO and formic acid.[14–18] However, for multi-carbon (C_{2+}) products, the performance in terms of current density, long-term stability, and especially product-specific selectivity still shows a considerable gap between the theoretical potential and numerous empirical outcomes.[19–22] Cu-based materials remain the only realistic catalysts for efficient C_{2+} production.[23–25] Furthermore, Cu-based bi-metallic catalysts have shown outstanding promise for the practical application of electrosynthesis of C_{2+} products in CO_2RR since Kenis *et al.*[26] and Jaramillo *et al.*[27] independently identified phase-dependent selective product for-mation and the now well-known tandem effect, respectively. However, advancing this field towards industrial applications

remains a significant challenge, as it is still in its early stages, with much progress yet to be made. The application of the tandem effect in Cu-based bimetallic catalysts for CO_2RR not only refines the adsorption and reaction pathways of the crucial intermediate CO, thereby enhancing its efficiency,[28–30] but also facilitates C–C coupling, increasing the probability of long-chain hydrocarbon formation and significantly boosting the selectivity for C_{2+} products.[31–33] A comprehensive understanding of the historical evolution of the tandem effect will offer critical perspectives for elucidating its structure–activity relationships at the catalyst surface/interface in catalytic processes.

In this review, we focus on Cu-based bimetallic catalysts for CO_2RR. Unlike other closely related reviews that focus on classifying the types, structures, and synthesis strategies of tandem catalysts, designing or predicting active structures based on the tandem effect, or summarizing prior research,[34–41] this review examines the tandem effect in Cu-based bimetallic catalysts. It identifies the most representative historical milestones in CO_2RR involving Cu-based bimetallic catalysts, outlines the underlying development patterns over the past decades, and finally highlights the foreseeable challenges in this field. In addition, numerous reviews have already provided an extensive discussion on the industrial and economic aspects of Cu-based catalysts for CO_2RR.[42–46] Therefore, our review focuses on the understanding and development of the catalytic process–surface/interface structure–activity relationships of Cu-based tandem catalysts for CO_2RR. We believe that this review can provide the research community with a clear and in-depth roadmap regarding Cu-based bimetallic catalysts for CO_2RR.

2. Early research in CO_2RR: metal-dependent product selectivity and crucial intermediate

2.1 The key classification of metal electrodes for CO_2RR

In the early research on CO_2RR, various metal electrodes were screened for their catalytic performance, providing numerous building block clues for the research community.[47–49] Importantly, in 1986, Hori firstly comprehensively summarized the previous trial-and-error. Innovatively, at that time, regardless of the poor understanding, he explicitly highlighted the element-dependent CO_2RR product selectivity and classified the metal electrodes regarding their product selectivity.[50,51] Specifically, his summary suggested that most common metal electrodes can be roughly classified into metals such as Au, Ag, and Zn that produce CO, metals such as Sn, In, and Pb that produce formic acid (or formate), metals such as Pt, Ti, Fe, and Ni that produce H_2, and the only metal, Cu, that generates both C_1 and C_{2+} products (Table 1). This classification not only establishes Cu as the only monometallic catalyst capable of facilitating the formation of both C_1 and C_{2+} products, thereby driving further exploration into C_{2+} production mechanisms, but also serves as a fundamental guideline for the strategic design of Cu-based tandem catalysts.

2.2 The CO intermediate for CO_2RR

To determine the fundamentals of the metal-dependent CO_2RR selectivity, Hori et al.,[52] in 1989, further examined the correlation between the potential and the selectivity for CO_2RR products on Cu electrodes. As shown in Fig. 1a, the faradaic efficiencies (FEs) of CO and formate were disclosed to have an

Table 1 CO_2 reduction products corresponding to different metal electrodes. Reprinted with permission from Hori et al.[50] Copyright 1994, Elsevier

Electrode	Potential vs. NHE	Current density (mA cm^{-2})	Faradaic efficiency (%)							
			CH_4	C_2H_4	EtOH	PrOH	CO	HCOO$^-$	H_2	Total
Cu	−1.44	5.0	33.3	25.5	5.7	3.0	1.3	9.4	20.5	103.5^a
Au	−1.14	5.0	0.0	0.0	0.0	0.0	87.1	0.7	10.2	98.0
Ag	−1.37	5.0	0.0	0.0	0.0	0.0	81.5	0.8	12.4	94.6
Zn	−1.54	5.0	0.0	0.0	0.0	0.0	79.4	6.1	9.9	95.4
Pd	−1.20	5.0	2.9	0.0	0.0	0.0	28.3	2.8	26.2	60.2
Ga	−1.24	5.0	0.0	0.0	0.0	0.0	23.2	0.0	79.0	102.0
Pb	−1.63	5.0	0.0	0.0	0.0	0.0	0.0	97.4	5.0	102.4
Hg	−1.51	0.5	0.0	0.0	0.0	0.0	0.0	99.5	0.0	99.5
In	−1.55	5.0	0.0	0.0	0.0	0.0	2.1	94.9	3.3	100.3
Sn	−1.48	5.0	0.0	0.0	0.0	0.0	7.1	88.4	4.6	100.1
Cd	−1.63	5.0	1.3	0.0	0.0	0.0	13.9	78.4	9.4	103.0
Tl	−1.60	5.0	0.0	0.0	0.0	0.0	0.0	95.1	6.2	101.3
Ni	−1.48	5.0	1.8	0.1	0.0	0.0	0.0	1.4	88.9	92.4^b
Fe	−0.91	5.0	0.0	0.0	0.0	0.0	0.0	0.0	94.8	94.8
Pt	−1.07	5.0	0.0	0.0	0.0	0.0	0.0	0.1	95.7	95.8
Ti	−1.60	5.0	0.0	0.0	0.0	0.0	tr.	0.0	99.7	99.7

Electrolyte: 0.1 M $KHCO_3$; temperature: 18.5 °C ± 0.5 °C. ^{a} The total value contains C_3H_5OH (1.4%), CH_3CHO (1.1%) and C_2H_5CHO (2.3%) in addition to the tabulated substances. ^{b} The total value contains C_2H_6 (0.2%).
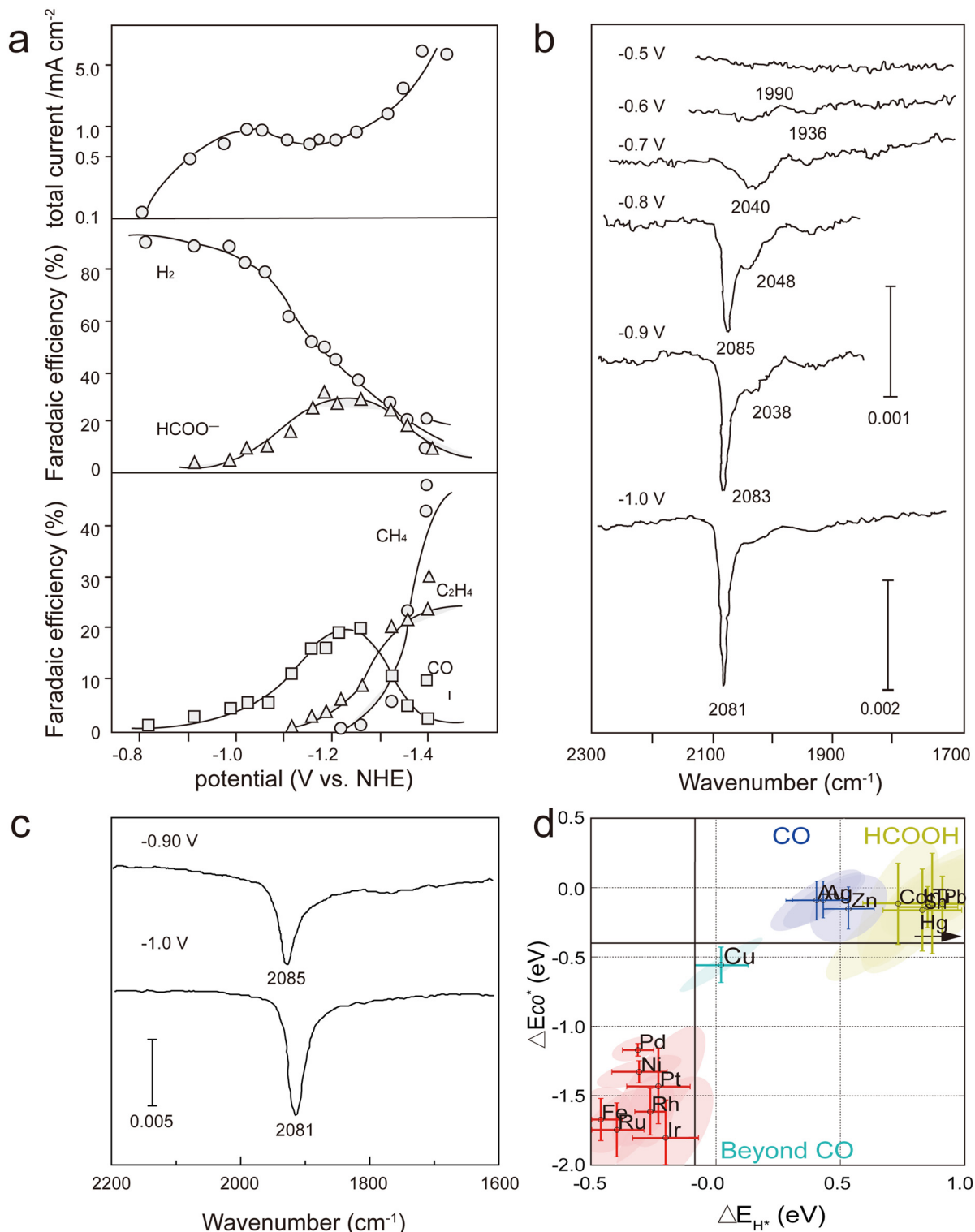
Fig. 1 (a) FE variations of CO_2 reduction products in 0.1 M $KHCO_3$ at 19 °C. (b) *In situ* IR spectra of adsorbed species on Cu during CO electroreduction at different potentials in 0.2 M $KHCO_3$. (c) *In situ* IR spectra of adsorbed species on Cu during CO_2 electroreduction at different potentials in 0.1 M $KHCO_3$. (d) *CO and *H binding energies set Cu apart from other metals. (a) Reprinted with permission from Hori *et al.*[52] Copyright 1989, the Royal Society of Chemistry. (b and c) Reprinted with permission from Hori *et al.*[56] Copyright 1995, Elsevier. (d) Reprinted with permission from Bagger *et al.*[60] Copyright 2017, John Wiley and Sons.

inverse correlation with that of CH_4 and C_2H_4, indicating that both CO and formate may be the crucial intermediates for the further reduced products. Evidently, CO was shown be reduced to CH_4 and C_2H_4 in other early studies.[53,54] However, when Cook et al.[55] directly and merely introduced formate into the electrolyte, they found that formate could not be reduced into any products such as CH_4, C_2H_4, and other multi-carbons. These experiments collectively indicate that CO should be the intermediate, instead of formate, which is further derived into other reduced products. Soon afterwards, Hori et al.[56] conclusively confirmed this deduction through in situ infrared spectroscopy during CO_2RR on a Cu electrode. As shown in Fig. 1b, a characteristic signal of CO adsorption emerged at 1900–2100 cm^{-1} when the potential reached −0.7 V vs. reversible hydrogen electrode (RHE). When CO_2 was replaced with CO, the in situ infrared spectra reproduced the CO binding signals observed in CO_2RR (Fig. 1c). Furthermore, metal electrodes such as Pt were then confirmed to have stronger CO binding strength, causing surface poisoning to occur and H_2 becomes the major product.[57] Reasonably, metal electrodes producing CO or formate were deduced to have a lower CO binding strength according to experimental results.[50,58,59] Since then, different metals have also been screened for their CO binding property, leading to the consensus that the CO binding strength on the metal surface is significant in terms of the CO_2RR product selectivity. Subsequently, an in-depth theoretical understanding was provided by Bagger et al.[60] As shown in Fig. 1d, the binding energies of CO* and H* (where * represents the adsorbed intermediates) were introduced as descriptors to explain the metal-dependent CO_2RR selectivity. This calculation aligns well with the previous deduction from experiments and conveys a vital message that *CO and *H bind neither too strong nor too weak on and only on the Cu surface, leading to the probability of C–C coupling[51] for the generation of C_{2+} products on Cu. These early studies on the metal-dependent CO_2RR selectivity and the identification of *CO as the key intermediate for C_{2+} products have laid the foundation for the recent development of Cu-based materials in CO_2RR. The pivotal role of *CO as the key intermediate in CO_2 reduction on the surface of Cu has been rigorously validated through both experimental evidence and theoretical calculations. This compelling confirmation has further stimulated extensive research interest, driving deeper exploration into this field.

3. Bimetallic Cu-based catalysts: the discovery of phase-dependent pathway and tandem effect

3.1 Breaking the scaling relationship on monometallic Cu-based materials by alloying

As discussed above, Cu-based materials are the only and most promising catalysts for CO_2RR to C_{2+} products, and thus significant research efforts have been devoted to Cu-based materials in

this field.[61–64] However, in the early stage, the performance of monometallic Cu was rather poor, largely due to the linear relationship between different adsorbed intermediates or the so-called scaling relationship (Fig. 2a).[65] This suggests that if a catalyst exhibits stronger binding strength to one intermediate, the binding strength to other intermediates is correspondingly enhanced, making it difficult to simultaneously achieve both high selectivity and high activity.[66,67] Thus, to break the scaling relationship and promote the selectivity as well as the activity, Nørskov et al.[65] theoretically proposed alloying Cu with a secondary metal to tune the binding strength or configuration of adsorbed intermediates on the catalyst surface. Thereafter, Cu-based bimetallic catalysts have become a focal point of research in this field, with researchers actively exploring their potential in enhancing the efficiency and selectivity of CO_2RR.[68–70] As expected, many bimetallic Cu-based catalysts showed a promoted performance compared to their monometallic counterparts. For instance, in 2014, Takanabe et al.[71] prepared a Cu–In alloy by in situ reducing Cu_2O in an $InSO_4$-containing electrolyte (Fig. 2b). The X-ray diffraction (XRD) patterns and elemental mapping of the Cu–In bimetallic alloy confirmed the formation of $Cu_{11}In_9$ featuring an In-rich surface and Cu-rich core. Moreover, $Cu_{11}In_9$ outperformed its oxide-derived Cu (OD-Cu) counterpart in terms of activity and selective CO production. Specifically, it was observed that OD-Cu primarily produces H_2 at −0.3 V vs. RHE, and as the potential becomes more negative, the products gradually shift to CO and HCOOH (Fig. 2c). In contrast, the $Cu_{11}In_9$ exhibits the highly efficient conversion of CO_2 to CO, while suppressing H_2 formation (Fig. 2d). Furthermore, Han et al.[72] developed a series of compositionally tunable Pd_xCu_y bimetallic aerogels using a template-free self-assembly approach. These aerogels, characterized by their three-dimensional porous architecture and high specific surface area, exhibited an exceptional electrocatalytic performance. Remarkably, they achieved an FE as high as 80.0% and a current density of 31.8 mA cm^{-2} for the electrochemical reduction of CO_2 to methanol, together with excellent stability under extended electrolysis conditions. Additionally, Huang et al.[73] developed a CuSn bimetallic catalyst with Cu and Sn uniformly distributed on its surface (Fig. 2e and f), which showed a superior selective formate production to monometallic Cu nanoparticles (Fig. 2g and h). Notably, numerous experimental reports also suggest that in bimetallic Cu-based catalysts, the secondary metal element largely impacts the final major product. Results show that when secondary metals are present in CO or formate producing metals, such as In, Sn, and Pd, bimetallic Cu-based materials predominantly produce CO[74,75] or formate,[76,77] while C_{2+} products are frequently generated on bimetallic CuAu, CuAg, and CuZn catalysts.[78–80] Typically, Ren et al.[80] developed a series of bimetallic CuZn catalysts ($Cu_{10}Zn$, Cu_4Zn, and Cu_2Zn) (Fig. 2i and j), finding that the doping level of Zn could effectively steer ethanol production, and the best Cu_4Zn catalyst exhibited a roughly 2-fold improvement in ethanol FE than its Cu counterpart (Fig. 2k and l). Additionally, Cao et al.[81] fabricated an $Ag–Cu_2O$ interfacial catalyst through a one-pot seed-mediated approach, which demonstrated an exceptional performance in the electrochemical
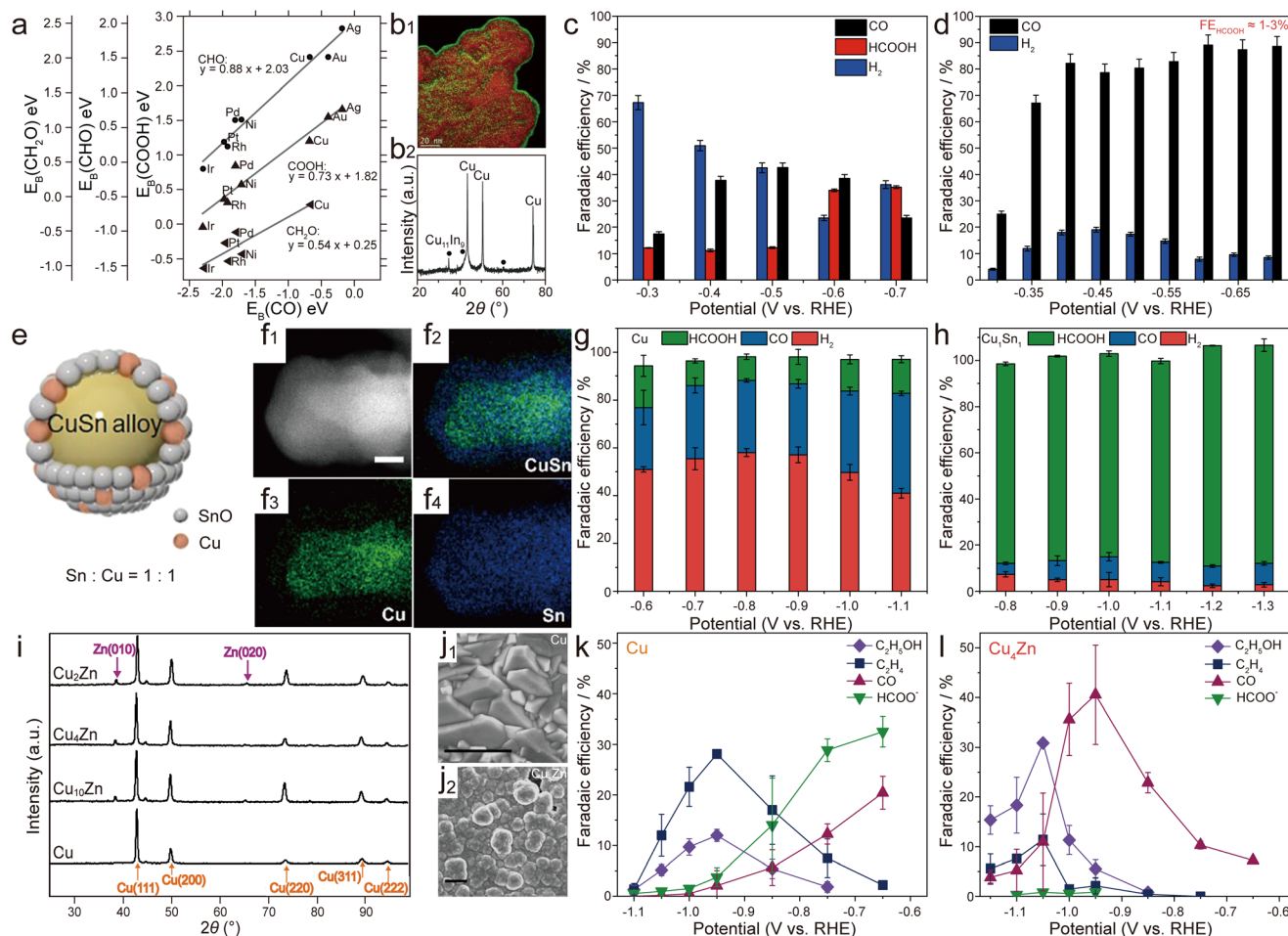
Fig. 2 (a) Linear relationships between different reaction intermediates (scaling relationships). (b_1 and b_2) EDS elemental mapping and XRD spectrum of Cu−In alloy, respectively. (c and d) FE of OD-Cu and Cu−In alloy for different products at various potentials, respectively. (e) Schematic of Cu−Sn alloy. (f_1–f_4) HAADF-STEM image and EDS elemental mapping of Cu−Sn alloy. Scale bar: 5 nm. (g and h) FE of different products for Cu and Cu_1Sn_1 alloy as a function of potential, respectively, with error bars representing the standard deviation from three independent measurements. (i) XRD patterns of Cu, $Cu_{10}Zn$, Cu_4Zn, and Cu_2Zn bimetallic catalysts. (j_1 and j_2) SEM images of Cu and the optimal catalyst Cu_4Zn, respectively. (k and l) FE of different products for Cu and Cu_4Zn alloy as a function of potential, respectively. (a) Reprinted with permission from Nørskov et al.[65] Copyright 2012, the American Chemical Society. (b and d) Reprinted with permission from Takanabe et al.[71] Copyright 2014, John Wiley and Sons. (e–h) Reprinted with permission from Huang et al.[73] Copyright 2021, the American Chemical Society. (i and l) Reprinted with permission from Ren et al.[80] Copyright 2016, the American Chemical Society.

reduction of CO_2 to C_2H_4 under neutral conditions. This catalyst achieved an impressive FE of 66.0% and a partial current density reaching 429.1 mA cm^{-2}. Insights from *in situ* Raman spectroscopy and theoretical calculations revealed that the Ag/Cu_2O interface effectively increases the *CO coverage and accelerates C–C coupling, thereby enhancing the generation of C_2H_4.

3.2 Phase-dependent CO_2RR on bimetallic Cu-based catalysts and tandem effect

Regardless of the fact that bimetallic CuAu, CuAg, and CuZn catalysts can selectively convert CO_2 into C_{2+} products, there was an interesting puzzle that bimetallic CuAu, CuAg, and CuZn catalysts do not always produce C_{2+} products.[82–86] As a classic example, in 2014, Yang et al.[87] prepared a group of homogeneous AuCu bimetallic nanoparticles with varying Au/Cu

ratios, which exhibited tunable selectivity, but merely generated CO, formate and H_2. Furthermore, Huang et al.[88] employed a two-step synthesis method to prepare CuAg nanowires (CuAgNWs) featuring atomic-scale Cu–Ag interfaces. These nanowires demonstrated remarkable selectivity toward methane (CH_4) in the electrochemical reduction of CO_2, achieving an impressive maximum FE of 72%. In parallel, Lim et al.,[89] through advanced density functional theory (DFT) calculations, highlighted the significant potential of the Cu_3Zn alloy catalyst for efficiently converting CO_2 into CH_4. These cases have brought widespread attention to the question of how to selectively generate C_{2+} products over bimetallic Cu-based catalysts. A milestone work conducted by Kenis et al.[26] directly addressed this puzzle by using CuPd catalysts with distinguished phases for the CO_2RR. As shown in Fig. 3a–c, three types of CuPd cata-

lysts, including phase-segregated, disordered solid solution, and atomically ordered phases, were prepared, respectively. Although their compositions are nearly identical, their phase differences caused selective C_{2+} production on phase-segregated CuPd nanoparticles, and dominant C_1 production on atomic ordered CuPd nanoparticles, respectively. Although the disordered CuPd nanoparticles enabled the catalytic production of both C_1 and C_{2+} with lower FEs than their other two counterparts (Fig. 3d). The phase-segregated CuPd intrinsically exhibited the properties of both monometallic Pd and Cu, and thus the CuPd nanoparticles did not significantly lower the d-band center, leading to the selective production of C_{2+}. Soon after, Jaramillo et al.[27] innovatively proposed the combination of metal producing CO and Cu to create a tandem effect. Specifically, an AuCu hybrid with phase-segregated state was utilized for the CO_2RR (Fig. 3e). Owing to the presence of Au and Cu components, which can effectively convert CO_2 to CO and CO to C_{2+}, the AuCu hybrid

electrode exhibited a large enhancement regarding the selective production of C_{2+} products compared to monometallic Cu (Fig. 3f and g). This tandem effect fundamentally takes advantages of Au nanoparticles for CO_2 reduction to CO, generating a high local concentration of CO on the adjacent Cu surface, where the migrated CO can be further reduced into C_{2+} products such as alcohols on the Cu surface. This work paves the way for the application of bimetallic Cu-based catalysts for C_{2+} production in CO_2RR, especially CuAu, CuAg, and CuZn, where the secondary metal characteristic is active for CO_2-to-CO conversion. As a supplementary to this finding, in 2019, Strasser et al.[90] extended the secondary metals to other components that can convert CO_2 into CO, such as Ni–N–C, which we now usually classify as metal–nitrogen–carbon based (M–N–C) materials.[91–94] The introduction of the tandem effect marks a groundbreaking advancement that has profoundly influenced the development of Cu-based bimetallic catalysts for CO_2RR, elevating research on
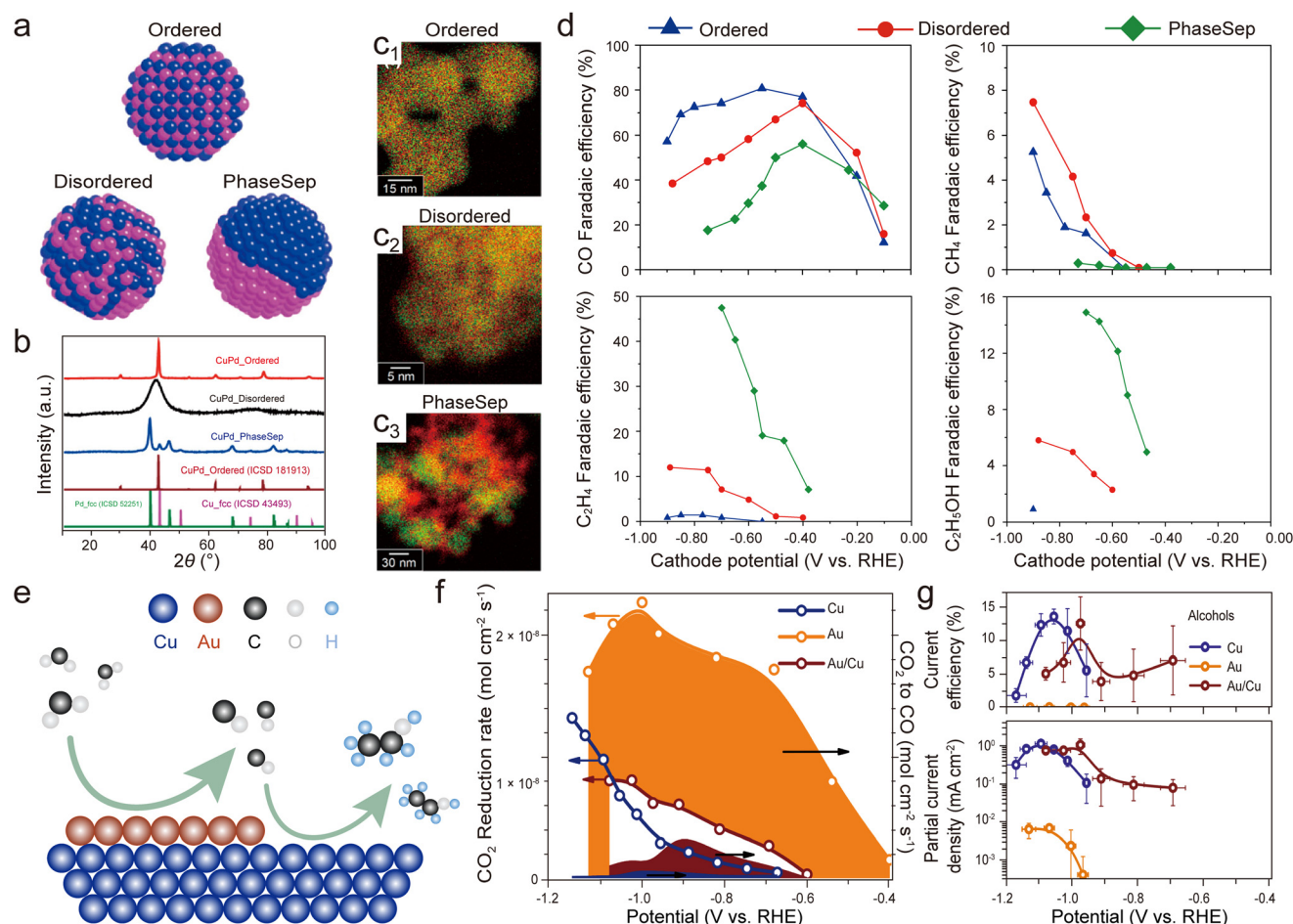
Fig. 3 (a and b) Schematic of Cu–Pd nanoalloys with ordered, disordered, and phase-separated structures, along with their corresponding XRD spectra. (c_1–c_3) EDS elemental mapping of three distinct Cu–Pd nanoalloys with ordered, disordered, and phase-separated structures, respectively, showing Cu (red) and Pd (green). (d) FEs of CO, CH_4, C_2H_4, and C_2H_5OH under three distinct structural configurations. (e) Schematic of CO_2RR over CuAu hybrid with a phase-separated state. (f) CO_2 consumption and CO_2 production rate as a function of applied potential. (g) Current efficiency and partial current density of alcohols in CO_2 reduction products corresponding to Cu, Au, and CuAu hybrids. (a–d) Reprinted with permission from Kenis et al.[26] Copyright 2017, the American Chemical Society. (f–g) Reprinted with permission from Jaramillo et al.[27] Copyright 2018, Springer Nature.

C_{2+} products to unprecedented levels. Following these pivotal discoveries, researchers began designing Cu-based bimetallic materials specifically to harness the advantages of the tandem effect, further advancing this field.[95–99] For instance, Yang *et al.*[95] prepared a CuAg tandem catalyst by physically mixing Cu and Ag nano-powders on a carbon paper substrate. Subsequently, this catalyst was employed in a gas diffusion flow cell for high-current CO_2 electrolysis, resulting in a C_{2+} current density of 160 mA cm^{-2} on the Cu surface. Moreover, the C_{2+} production rate was four times higher than that of pure Cu. Moreover, Shen *et al.*[100] employed an enhanced polyethylene glycol method combined with subsequent electrochemical reduction to fabricate Ag–Cu bimetallic surface alloys with adjustable surface chemical compositions, varying from Cu-rich to Ag-rich. These materials exhibited tunable product selectivity in the electrochemical reduction of CO_2, presenting an innovative approach for developing catalysts with precisely controlled product outcomes. This breakthrough provides promising prospects for improving the efficiency of industrial CO_2 conversion and utilization. Also, these remarkable results further underscore the industrial potential of the tandem effect.

4. Tandem effect is still not perfect

4.1 Reactor/cell design to address the problems of CO utilization and potential misalignment in tandem effect

The finding of the tandem effect based on phase segregation in bimetallic Cu-based catalysts has significantly propelled the advancements in this field. Nevertheless, this does not mean that the tandem effect is the ultimate solution of CO_2RR. Usually, if we merely combine CO-producing metals/components (*e.g.*, Ag, Au, and Zn or M–N–C) and Cu, the production of C_{2+} can be promoted to a great extent. However, the C_{2+} promotion in previous reports are not all satisfactory.[101–104]

As a matter of fact, two important issues have been encountered with the tandem effect. The first issue is CO utilization. Looking carefully at the scenario of CO_2RR on bimetallic Cu-based catalysts, there is still an open question of can the CO generated on Au, for example, can be fully used for further reduction on Cu? Or will the CO generated initially flash through the cell before it can effectively bind on the Cu surface? The outcome probably is concerning, as evidenced by the CO production rate or partial current density of CO in previous bimetallic Cu-based systems.[105–107] Thus, to address this concern, Wu *et al.*[108] recently designed a segmented gas diffusion electrode (s-GDE) (Fig. 4a). In the fabrication of s-GDE, firstly uniform Cu catalyst layer (CL) segments were applied on the GDE, working as C_{2+} selective segments. Then, Ag CL segments were concentrated near the inlet, functioning as the CO selective segments. The area and positioning of the Ag CL segments were precisely controlled by a template. The CO-selective (Ag) CL segment near the inlet extended the retention time of CO in the subsequent C_{2+} selective (Cu) segments, thus enhancing the utilization of CO and final C_{2+} production (Fig. 4b). This tiny change brought about a significant difference.

Besides the CO utilization issue, the other problem of tandem effect regarding C_{2+} promotion is the potential misalignment. Specifically, the optimal potential for CO_2-to-CO
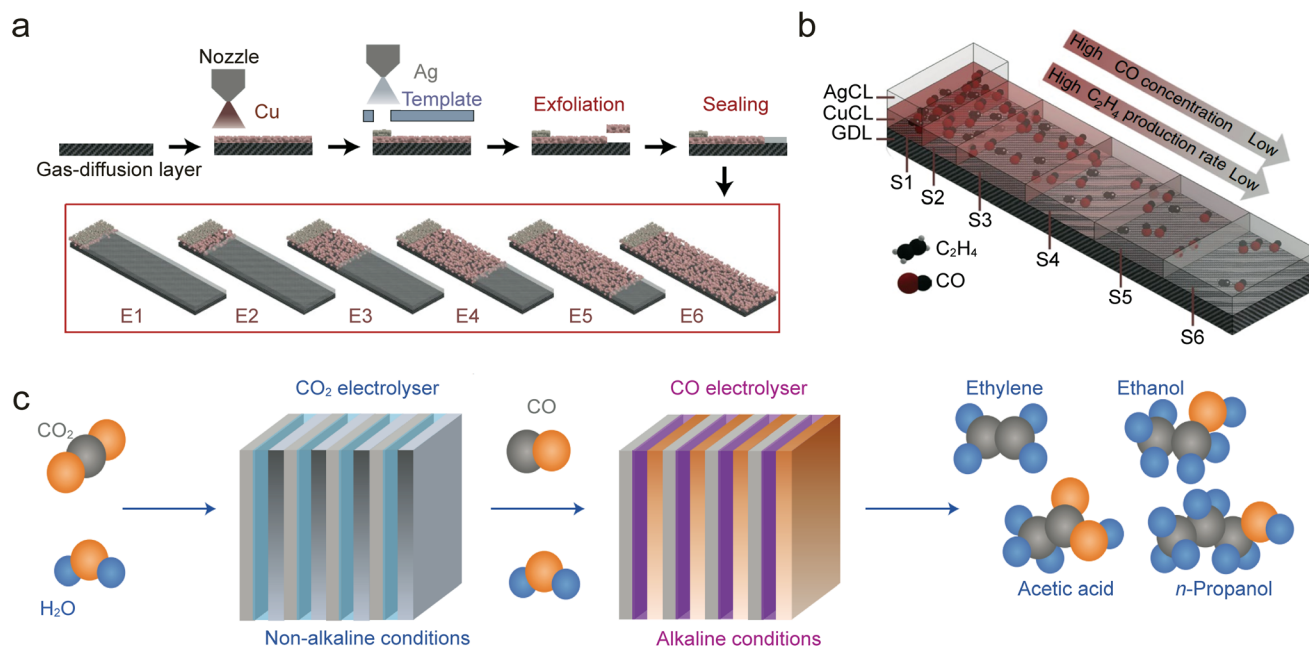
Fig. 4 (a) Schematic of the s-GDE preparation process, showing the geometries of six s-GDEs (from E_1 to E_6), where the Ag catalyst layer (CL) size is constant, while the Cu catalyst layer size varies. (b) Schematic of the reduction in C_{2+} mass activity and CO concentration. (c) Schematic of the two-step electrolysis process for converting CO_2 into C_{2+} products using CO_2 and H_2O as reactants. (a and b) Reprinted with permission from Zhang *et al.*[108] Copyright 2022, Springer Nature. (c) Reprinted with permission from Jiao *et al.*[110] Copyright 2019, Springer Nature.

conversion on the secondary component in most cases does not match well with the optimal potential for the CO-to-C_{2+} process on Cu. This issue can be partially addressed by rationally designing catalyst pairs (Cu and a secondary CO-producing component) that share a mutual optimal electrochemical window. For example, Liu et al.[109] demonstrated this approach with their Ni single-atom-catalyst/Cu-R (R for reduction state) hybrid. However, this technique typically requires extensive trial-and-error. This circumstance makes it challenging to push the tandem effect to its ideal promotion limit. Therefore, in 2019, Jiao et al.[110] proposed an unprecedented alternative solution by using a divided cell system, where the CO_2-to-CO and CO-to-C_{2+} processes can be operated in two cells independently. Basically, the first cell can use CO-producing catalysts such as Ag, Au, Zn, and M–N–C catalysts, while CO is fed as a cascade in the second cell equipped with Cu catalysts (Fig. 4c). Our group[111] even demonstrated that with this strategy, the not only the total C_{2+} production could be improved, the specific C_{2+} product (acetate in our case) could also be custom-tailored via facile selection of the Cu catalyst. Employing this divided cell system, the potential misalignment can be largely alleviated. Another bonus of this system should be the promising promotion of carbon efficiency and current density by custom-tailoring the electrolyte pH in each cell. This is because acidic and alkaline electrolytes have been well studied as the optimal condition for CO_2 utilization and CO reduction, respectively.[112–115] As previously discussed, the electrolyte is a crucial factor influencing the CO_2RR performance. Thus, to explore this aspect, our group[116] conducted experiments, which revealed that during the electrochemical CO_2 reduction reaction, the $Cu^{\delta+}$ species on the surface of OD-Cu undergo dynamic reduction and reoxidation in $KHCO_3$ electrolyte due to the presence of hydroxyl radicals ($^{\bullet}OH$). Based on these findings, we proposed the "seesaw effect" to elucidate the dynamic equilibrium of the $Cu^{\delta+}$ chemical states and concentrations, further underscoring the pivotal role of electrolyte composition in governing the CO_2RR performance. Leveraging the tandem effect to optimize the reactor/cell design not only offers significant advantages in enhancing the selectivity and catalytic activity for C_{2+} products but also presents new opportunities for exploring its industrial feasibility. By precisely regulating the reaction microenvironment, this strategy holds great promise for overcoming existing technological bottlenecks, further improving the energy conversion efficiency and accelerating the industrialization of CO_2RR, ultimately enabling large-scale and stable production.

4.2 Pushing the understanding limit beyond the tandem effect regarding detailed product

According to the discussion above, it is well recognized that the total C_{2+} production benefits from the tandem effect. However, the tandem effect theory fails when we investigated in detail the single C_{2+} product. In many works employing bimetallic Cu-based catalysts having close or even identical components, their reported C_{2+} products in CO_2RR exhibited a totally different distribution for ethylene, ethanol, acetate,

and/or n-propanol.[117–122] Taking CuAg catalysts as an example, Grätzel et al.[117] fabricated CuAg bimetallic tandem catalysts through the electrochemical substitution of Cu(I) ions in Cu_2O nanowires with Ag(I) ions from an $AgNO_3$ solution. Alternatively, Sargent et al.[118] prepared CuAg tandem catalysts by co-sputtering Cu and Ag on a polytetrafluoroethylene (PTFE) substrate. These two approaches have led to an improvement in the selective production of ethylene (with an FE of 52% at −1.05 V vs. RHE) and ethanol (with a FE of 41% at −0.67 V vs. RHE), respectively. This sort of phenomena cannot be easily understood/explained by merely the tandem effect theory. The observed disparities in C_{2+} product distribution can be attributed to the structural characteristics in the catalyst. In particular, the facet orientation in Cu-based catalysts plays a crucial role in determining the product selectivity. For instance, Cu (100) facets are reported to favor C–C coupling, leading to enhanced ethylene production, whereas Cu (111) facets promote oxygenate formation, resulting in increased ethanol yields.[123] In addition to catalyst structure, external reaction conditions also play a pivotal role in modulating the C_{2+} product selectivity. Specifically, the applied potential plays a pivotal role in modulating the adsorption and activation of CO_2, thereby exerting a significant influence on product selectivity in CO_2RR. At lower potentials, CO_2 adsorption and activation are more favorable, leading to an increased CO yield. In contrast, higher potentials tend to promote the hydrogen evolution reaction (HER), which competes with CO_2RR, and ultimately diminishes its selectivity.[124] Furthermore, we hypothesize that this discrepancy may arise from the intrinsic susceptibility of Cu-based catalysts to oxidation, leading to the formation of surface or bulk oxides/oxide layers during their synthesis or storage. Upon reduction, these oxides undergo reconstruction, creating new active sites, commonly referred to as OD-Cu. In this reconstruction process, the secondary metal or other components may exert a significant influence on the behavior and properties of the reconstructed sites.[125] Accordingly, investigating the reconstruction behavior of OD-Cu is imperative and should not be neglected.

This fundamental puzzle also has driven research attention to further determine the mechanism (or structure–performance correlation) beyond the tandem effect. To obtain an in-depth understanding of the structure-dependent impact of bimetallic Cu-based catalysts on their CO_2RR performance, Buonsanti et al.[126] selected CuAg as a platform and synthesized three CuAg bimetallic nanodimers (NDs) with different Cu/Ag inter-contacting areas ($Ag_1Cu_{0.4}$ NDs, $Ag_1Cu_{1.1}$ NDs, and $Ag_1Cu_{3.2}$ NDs) for CO_2RR (Fig. 5a). As expected based on the tandem effect, a physical mixture of Ag NPs and Cu NPs used as an electrocatalyst for CO_2RR exhibited a 1.5-fold FE for C_2H_4 compared to that of Cu NPs alone (Fig. 5b). However, surprisingly, the CuAg bimetallic NDs did not show a superior C_2H_4 FE than its mixture counterpart or even Cu NPs (Fig. 5b), directly reflecting something plays a role beyond the tandem effect. According to the XPS profiles of CuAg NDs, the authors proposed that as the Cu domain size increases, the binding
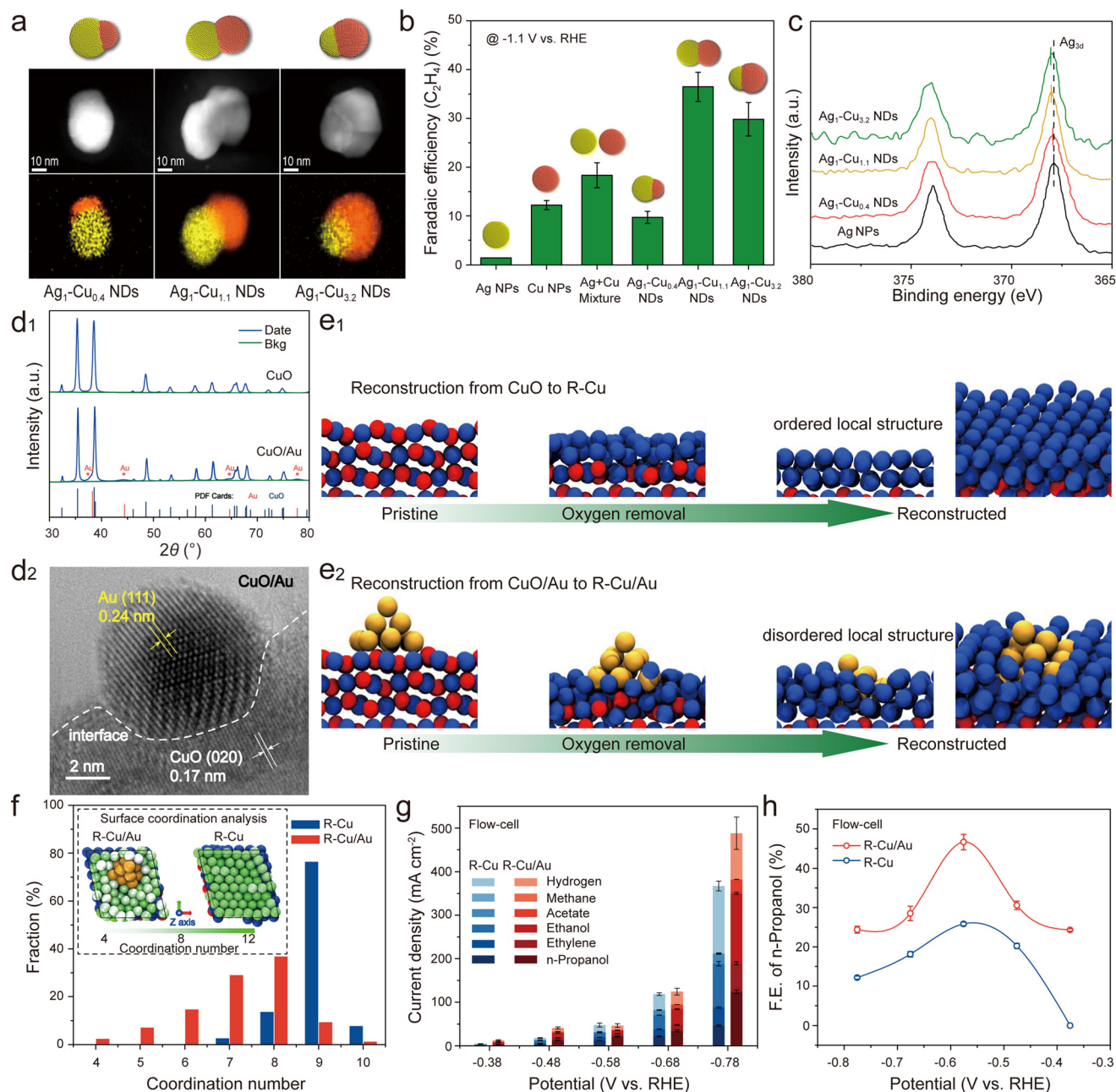
Fig. 5 (a) Schematic, HAADF-STEM images, and corresponding EDS elemental mappings of three Ag–Cu NDs, showing Cu (orange) and Ag (yellow). (b) FE of C_2H_4 obtained on three different Ag–Cu NDs, with error bars representing the standard deviation from at least three independent measurements. (c) XPS spectra of three different Ag–Cu NDs. (d_1 and d_2) XRD patterns of CuO and CuO/Au, with PDF cards corresponding to Au (No. 65-8601) and CuO (No. 80-1916), along with the HR-TEM image of CuO/Au, respectively. (e_1 and e_2) Snapshots of the simulated reconstruction process from CuO to R–Cu and from CuO/Au to R–Cu/Au, respectively. Cu (blue), O (red), Au (yellow). (f) Analysis of surface Cu coordination environments in R–Cu and R–Cu/Au systems, with statistical distribution of coordination numbers. Dark/light green indicate Cu atoms with distinct coordination states, yellow denotes Au atoms. (g and h) Partial current densities of different CORR products and the FE of n-propanol on R–Cu/Au and R–Cu in a flow cell with CO-saturated 1.0 M KOH as the electrolyte, respectively. (a–c) Reprinted with permission from Buonsanti et al.[126] Copyright 2019, the American Chemical Society. (d–h) Reprinted with permission from Cui et al.[129] Copyright 2024, the American Chemical Society.

energy of Ag_{3d} in the Ag–Cu ND is continuously blue-shifted, indicating that the transfer of electrons from the Cu domain to the Ag domain will dominantly steer the final pathway to C_2H_4 (Fig. 5c). Moreover, considering that Cu-based materials always undergo reconstruction under electrocatalysis,[127,128] naturally

researchers suspect that the secondary metal probably influences the reconstruction of the Cu component during the reaction. Thus, to test this hypothesis, more recently, our group[129] employed a CuO/Au hybrid as a platform to investigate the reconstruction behavior of Cu-based components when deco-

rated with/without Au (Fig. 5d). Interestingly, it was found that the local Cu atoms surrounding Au tended to rearrange into disordered layers, rather than forming the densely packed Cu (111) plane observed on bare CuO (Fig. 5e). Meanwhile, the disordered Cu species near Au in the reconstructed Cu/Au exhibited abundant undercoordinated atoms compared to the reconstructed Cu (Fig. 5f). Consequently, these undercoordinated Cu sites boost the selective electrosynthesis of n-propanol (Fig. 5g and h). In addition, our group[130] investigated the reconstruction behavior of OD-Cu in electrochemical CO_2 reduction through molecular dynamics simulations and experimental studies. We found that Cu derived from CuO (CuOD-Cu) exhibits a higher density of low-coordinated Cu sites and greater surface Cu atom density compared to Cu derived from Cu_2O (Cu_2OD-Cu). As a result, CuOD-Cu demonstrated a superior FE for n-propanol in CO_2RR, reaching up to 17.9%. These three representative works may inspire more efforts for the understanding beyond the tandem effect theory.

5. Conclusion and outlooks

In this review, we comprehensively and insightfully summarized the historical development of the tandem effect in Cu-based bimetallic CO_2 reduction. We covered its origin, relevant

applications, and in-depth exploration of its limitations (Fig. 6). The discovery of the tandem effect has significantly transformed the challenges of low selectivity, poor yield, and high overpotential in electrochemical CO_2 reduction to C_{2+} products. This has laid a theoretical foundation for achieving stable CO_2 conversion into C_2, C_3, and even higher-order carbon-based products. Although the large-scale industrial implementation of the tandem effect is presently limited by technological and economic challenges, it remains a highly promising strategy for C_{2+} production, with the potential to revolutionize traditional industrial processes. With continued technological advancements and progressive cost reductions, the tandem effect is poised to play a transformative role in future industrial applications. Given the critical role of electrochemical CO_2 reduction in addressing climate change and facilitating the transition to sustainable energy, research in this field is of paramount urgency and significance. However, greater emphasis on economic viability will be essential in future industrial adoption to ensure that it not only drives the green energy transition and achieves carbon neutrality goals but also delivers tangible commercial value. In future industrial applications, although Cu is relatively inexpensive, the use of noble metals as secondary components will inevitably increase the overall cost. Thus, minimizing the dependence on noble metals will be crucial for ensuring economic feasibility.
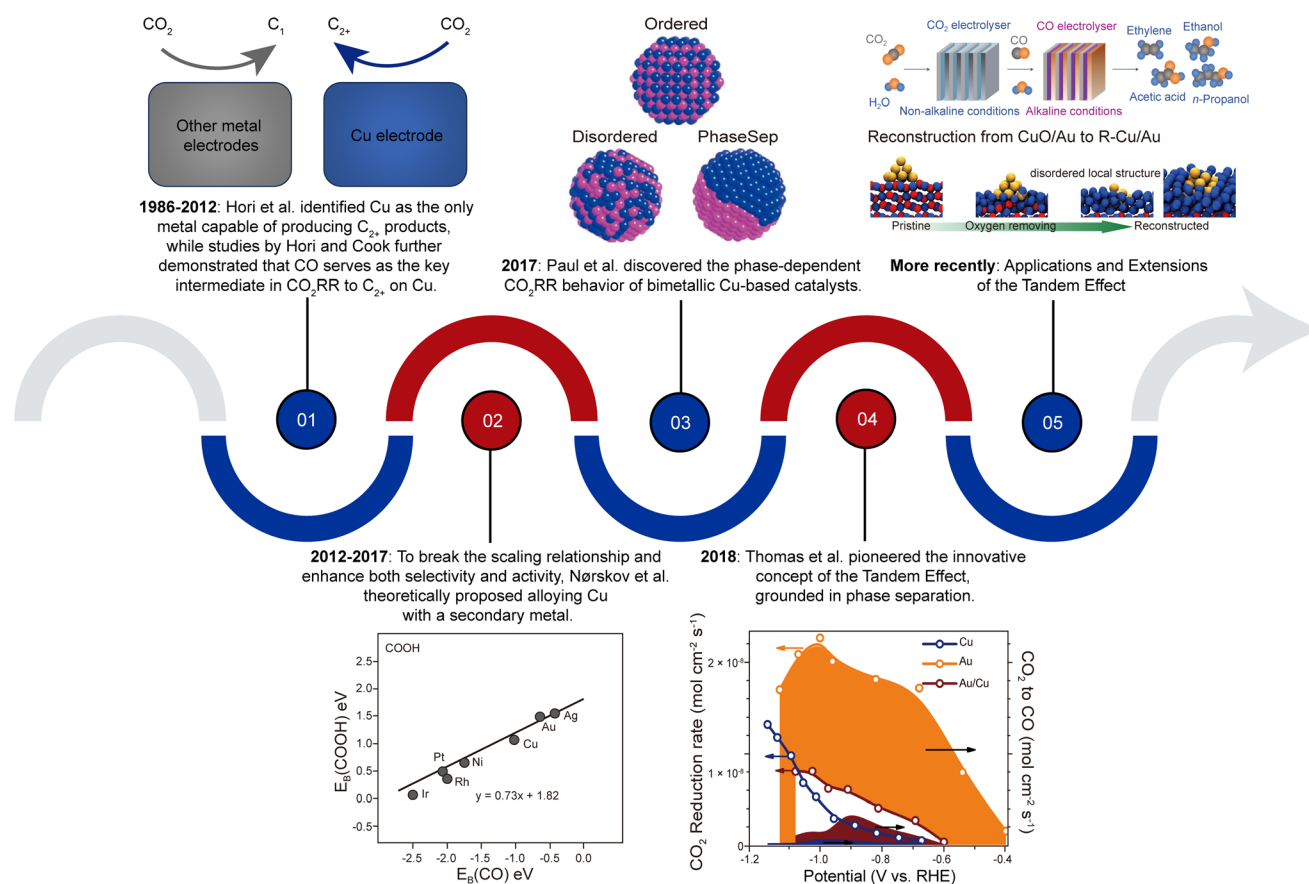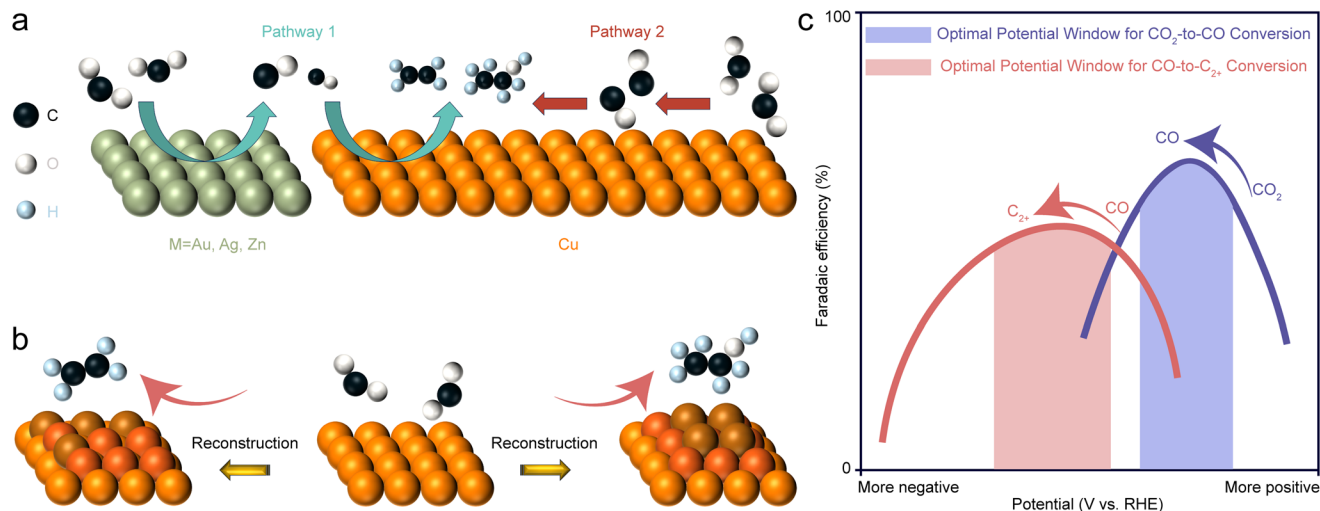

Fig. 6 Schematic of the milestones in the historical development of the tandem effect.

Fig. 7 Advancing Cu-based bimetallic catalysts for optimizing the tandem effect in CO_2RR: future research directions: (a) generation and utilization of CO: sources and pathways. (b) Cu reconstruction and tailoring of product selectivity. (c) Disparity and misalignment in electrochemical potential windows for CO_2-to-CO and CO-to-C_{2+} pathways.

Additionally, tandem reactors can significantly improve the CO_2 utilization, enhancing CO production under acidic conditions and increasing the current density for CO to C_{2+} conversion under alkaline conditions. However, each additional reactor unit increases the system costs, which can present a substantial economic challenge for large-scale implementation. In addition to the aforementioned aspects, factors such as catalyst stability,[131] energy efficiency,[132] loading strategy,[133] and reaction conditions[134] also play crucial roles in influencing the performance of the tandem effect. These factors interact synergistically, collectively determining the manifestation of the tandem effect in the CO_2RR process, as well as the selectivity and conversion efficiency of the final products. Furthermore, based on our in-depth evaluation of the fundamental underlying mechanisms for the tandem effect, we have identified two critical challenges in its application that demand further resolution and optimization. Firstly, the efficient utilization of CO intermediates for conversion to C_{2+} products, which represents a key bottleneck in achieving high catalytic efficiency based on this effect. The efficiency of CO intermediate conversion is not only dependent on the activity of the catalytic sites but also closely linked to the stability of the intermediates on the catalyst surface. Addressing this challenge will require the development of catalyst systems capable of effectively modulating CO adsorption and desorption behaviors. In particular, precise control of the reaction pathways of the CO intermediates on the surface of copper is anticipated to be a focal point for future research efforts. Secondly, the potential mismatch between Cu and the secondary metal is another critical factor that merits attention. This potential mismatch may adversely affect the overall performance of the catalyst, specifically by constraining the efficient conversion of CO intermediates on its surface and hindering the effective formation of C_{2+} products. Consequently, this diminishes the

synergistic effects inherent to the bimetallic system, further limiting its catalytic efficiency. Additionally, we attributed the observed differences in the distribution and trends of deep reduction products, even among Cu-based bimetallic systems with similar or identical compositions, to the reconstruction of Cu induced by the second metal. This reconstruction alters the product distribution and remains an area where the detailed mechanisms require further investigation. Here, we outlook several key scientific questions that merit deeper exploration in future research (Fig. 7).

1. In Cu-based bimetallic CO_2RR, is all the CO generated by the secondary metal utilized for further reduction to C_{2+} products on Cu? Can this be quantitatively analyzed? Alternatively, does all the CO involved in deep reduction on Cu originate exclusively from the CO_2 reduction occurring on the secondary metal?

2. There exists a significant potential mismatch between the optimal potentials for CO generation by the secondary metal and the deep reduction of CO to C_{2+} products by Cu, resulting in insufficient tandem effect gains. Besides exploring catalysts with broad potential windows, can the optimal potentials for both processes be aligned through external environmental adjustments?

3. There is currently no unified theory on how the introduction of a secondary metal induces Cu reconstruction and does this reconstruction favorably influence the selectivity toward C_{2+} products?

Author contributions

C. L. and F. D. obtained financial support. C. L. conceptualized and supervised the project. D. L. and C. L. drafted the

manuscript. W. D. and D. L. visualized the figures. All authors commented on and edited the manuscript.

Data availability

No primary research results, software or code have been included and no new data were generated or analyzed as part of this review.

Conflicts of interest

There are no conflicts to declare.

Acknowledgements

References

1 C. Long, X. Li, J. Guo, Y. N. Shi, S. Q. Liu and Z. Y. Tang, *Small Methods*, 2018, **3**, 1800369.

2 J. B. Huang, X. P. Zhang, J. Yang, J. M. Yu, Q. J. Chen and L. S. Peng, *Adv. Sci.*, 2024, **11**, 2309865.

3 Z. W. Seh, J. Kibsgaard, C. F. Dickens, I. Chorkendorff, J. K. Nørskov and T. F. Jaramillo, *Science*, 2017, **355**, eaad4998.

4 F. Wang, J. D. Harindintwali, Z. Z. Yuan, M. Wang, F. Wang, S. Li, Z. G. Yin, L. Huang, Y. Fu, L. Li, S. X. Chang, L. J. Zhang, J. Rinklebe, Z. Q. Yuan, Q. G. Zhu, L. L. Xiang, D. C. W. Tsang, L. Xu, X. Jiang, J. H. Liu, N. Wei, M. Kastner, Y. Zou, Y. S. Ok, J. L. Shen, D. L. Peng, W. Zhang, D. Barcelo, Y. J. Zhou, Z. H. Bai, B. Q. Li, B. Zhang, K. Wei, H. J. Cao, Z. L. Tan, L. B. Zhao, X. He, J. X. Zheng, N. Bolan, X. H. Liu, C. P. Huang, S. Dietmann, M. Luo, N. N. Sun, J. R. Gong, Y. L. Gong, F. Brahushi, T. T. Zhang, C. D. Xiao, X. F. Li, W. F. Chen, N. Z. Jiao, J. Lehmann, Y. G. Zhu, H. G. Jin, A. Schäffer, J. M. Tiedje and J. M. Chen, *Innovation*, 2021, **2**, 100180.

5 J. Li, H. C. Xiong, X. Z. Liu, D. H. Wu, D. Su, B. J. Xu and Q. Lu, *Nat. Commun.*, 2023, **14**, 698.

6 Y. Kong, H. P. Yang, X. M. Jia, D. Wan, Y. L. Zhang, Q. Hu and C. X. He, *Nano Lett.*, 2024, **24**, 9345–9352.

7 J. M. Spurgeon and B. Kumar, *Energy Environ. Sci.*, 2018, **11**, 1536–1551.

8 S. Kumar De, D. I. Won, J. Kim and D. H. Kim, *Chem. Soc. Rev.*, 2023, **52**, 5744–5802.

9 T. Alerte, A. Gaona, J. P. Edwards, C. M. Gabardo, C. P. O'Brien, J. Wicks, L. Bonnenfant, A. S. Rasouli, D. Young, J. Abed, L. Kershaw, Y. C. Xiao, A. Sarkar, S. A. Jaffer, M. W. Schreiber, D. Sinton, H. L. MacLean and

E. H. Sargent, *ACS Sustainable Chem. Eng.*, 2023, **11**, 15651–15662.

10 T. R. Wei, S. S. Zhang, Q. Liu, Y. Qiu, J. Luo and X. J. Liu, *Acta Phys.-Chim. Sin.*, 2023, **39**, 202207026.

11 S. S. Gao, T. W. Wang, M. M. Jin, S. S. Zhang, Q. Liu, G. Z. Hu, H. Yang, J. Luo and X. J. Liu, *Sci. China Mater.*, 2023, **66**, 1013–1023.

12 J. Y. Ding, T. R. Wei, T. Hou, W. J. Liu, Q. Liu, H. Zhang, J. Luo and X. J. Liu, *Nanoscale*, 2024, **16**, 10628–10636.

13 G. R. Zhang, B. Tan, D. H. Mok, H. Y. Liu, B. X. Ni, G. Zhao, K. Ye, S. J. Huo, X. H. Miao, Z. Liang, X. Liu, L. W. Chen, Z. M. Zhang, W. B. Cai, S. Back and K. Jiang, *Proc. Natl. Acad. Sci. U. S. A.*, 2024, **121**, e2400898121.

14 S. Jin, Z. M. Hao, K. Zhang, Z. H. Yan and J. Chen, *Angew. Chem., Int. Ed.*, 2021, **60**, 20627–20648.

15 X. J. She, Y. F. Wang, H. Xu, S. C. E. Tsang and S. P. Lau, *Angew. Chem., Int. Ed.*, 2022, **61**, e202211396.

16 W. G. Zhao and T. Wang, *ACS Catal.*, 2024, **14**, 8549–8560.

17 J. Yin, J. Jin, Z. Y. Yin, L. Zhu, X. Du, Y. Peng, P. X. Xi, C. H. Yan and S. H. Sun, *Nat. Commun.*, 2023, **14**, 1724.

18 J. H. Bi, P. S. Li, J. Y. Liu, Y. Wang, X. N. Song, X. C. Kang, X. F. Sun, Q. G. Zhu and B. X. Han, *Angew. Chem., Int. Ed.*, 2023, **62**, e202307612.

19 M. Jouny, W. Luc and F. Jiao, *Ind. Eng. Chem. Res.*, 2018, **57**, 2165–2177.

20 J. Na, B. Seo, J. Kim, C. W. Lee, H. Lee, Y. J. Hwang, B. K. Min, D. K. Lee, H. S. Oh and U. Lee, *Nat. Commun.*, 2019, **10**, 5193.

21 P. Zhu and H. T. Wang, *Nat. Catal.*, 2021, **4**, 943–951.

22 E. Ruiz-López, J. Gandara-Loe, F. Baena-Moreno, T. R. Reina and J. A. Odriozola, *Renewable Sustainable Energy Rev.*, 2022, **161**, 112329.

23 Y. Hori, K. Kikuchi, A. Murata and S. Suzuki, *Chem. Lett.*, 1986, **15**, 897–898.

24 J. C. Bui, C. Kim, A. J. King, O. Romiluyi, A. Kusoglu, A. Z. Weber and A. T. Bell, *Acc. Chem. Res.*, 2022, **55**, 484–494.

25 M. H. Jiang, H. Z. Wang, M. F. Zhu, X. J. Luo, Y. He, M. J. Wang, C. J. Wu, L. Y. Zhang, X. Li, X. M. Liao, Z. J. Jiang and Z. Jin, *Chem. Soc. Rev.*, 2024, **53**, 5149–5189.

26 S. C. Ma, M. Sadakiyo, R. Heima, R. Luo, R. T. Haasch, J. I. Gold, M. Yamauchi and P. J. A. Kenis, *J. Am. Chem. Soc.*, 2017, **139**, 47–50.

27 C. G. Morales-Guio, E. R. Cave, S. A. Nitopi, J. T. Feaster, L. Wang, K. P. Kuhl, A. Jackson, N. C. Johnson, D. N. Abram, T. Hatsukade, C. Hahn and T. F. Jaramillo, *Nat. Catal.*, 2018, **1**, 764–771.

28 J. J. Li, Y. Chen, B. Q. Yao, W. J. Yang, X. Y. Cui, H. L. Liu, S. Dai, S. B. Xi, Z. Y. Sun, W. X. Chen, Y. C. Qin, J. L. Wang, Q. He, C. Y. Ling, D. S. Wang and Z. C. Zhang, *J. Am. Chem. Soc.*, 2024, **146**, 5693–5701.

29 J. J. Fu, H. N. Zhang, H. T. Du, X. Z. Liu, Z. H. Lyu, Z. Jiang, F. R. Chen, L. Ding, T. Tang, W. L. Zhu, D. Su, C. Y. Ling, J. L. Wang and J. S. Hu, *J. Am. Chem. Soc.*, 2024, **146**, 23625–23632.

30 G. Y. Zhou, B. Y. Li, G. M. Cheng, C. J. Breckner, D. P. Dean, M. Q. Yang, N. Yao, J. T. Miller, J. B. M. Klok, N. Tsesmetzis, G. F. Wang and Z. J. Ren, *J. Am. Chem. Soc.*, 2024, **146**, 31788–31798.

31 Z. Y. Wen, M. J. Wang, C. L. Liang, B. J. Fan, Y. C. Yan, J. Fan, N. Han, Y. H. Wang and Y. G. Li, *J. Am. Chem. Soc.*, 2024, **146**, 32575–32581.

32 Y. Long, Z. J. Chen, L. Wu, X. Q. Liu, Y. N. Hou, S. Vernuccio, W. Wei, W. Y. Wong and B. J. Ni, *Small Sci.*, 2024, **4**, 2400129.

33 P. F. Sui, Y. C. Wang, X. L. Wang, S. B. Liu and J. L. Luo, *ChemCatChem*, 2024, e202401604.

34 A. Vasileff, C. C. Xu, Y. Jiao, Y. Zheng and S. Z. Qiao, *Chem*, 2018, **4**, 1809–1831.

35 D. F. Gao, R. M. Arán-Ais, H. S. Jeon and B. R. Cuenya, *Nat. Catal.*, 2019, **2**, 198–210.

36 C. L. Xiao and J. Zhang, *ACS Nano*, 2021, **15**, 7975–8000.

37 B. Cao, F. Z. Li and J. Gu, *ACS Catal.*, 2022, **12**, 9735–9752.

38 Y. F. Jia, F. Li, K. Fan and L. C. Sun, *Adv. Powder Mater.*, 2022, **1**, 100012.

39 X. Q. Wang, Q. Chen, Y. J. Zhou, H. M. Li, J. W. Fu and M. Liu, *Adv. Sen. Energy Mater.*, 2022, **1**, 100023.

40 Q. Q. Qing, H. L. Suo, L. J. Chen, Y. X. Wang, J. Z. Wang, H. K. Liu, S. X. Dou, M. M. Lao and W. H. Lai, *Adv. Mater. Interfaces*, 2024, **11**, 2301049.

41 P. Q. Guo, K. L. Liu, X. Liu, R. H. Liu and Z. Y. Yin, *Energy Fuels*, 2024, **38**, 5659–5675.

42 J. M. Spurgeon and B. Kumar, *Energy Environ. Sci.*, 2018, **6**, 1536–1551.

43 D. Tian, Z. G. Qu and J. F. Zhang, *Appl. Energy*, 2023, **351**, 121787.

44 R. Haaring, P. W. Kang, Z. M. Guo, J. W. Lee and H. Lee, *Acc. Chem. Res.*, 2023, **56**, 2595–2605.

45 S. Varhade, A. Guruji, C. Singh, G. Cicero, M. G. Melchor, J. Helsen and D. Pant, *ChemElectroChem*, 2024, e202400512.

46 A. Al Moinee, A. A. Rownaghi and F. Rezaei, *Chem. Eng. J.*, 2024, **499**, 155909.

47 W. L. Zhu, R. Michalsky, Ö. Metin, H. Lv, S. J. Guo, C. J. Wright, X. L. Sun, A. A. Peterson and S. Sun, *J. Am. Chem. Soc.*, 2013, **135**, 16833–16836.

48 A. D. Castillo, M. Alvarez-Guerra, J. Solla-Gullón, A. Sáez, V. Montiel and A. Irabien, *Appl. Energy*, 2015, **157**, 165–173.

49 D. F. Gao, H. Zhou, J. Wang, S. Miao, F. Yang, G. X. Wang, J. G. Wang and X. H. Bao, *J. Am. Chem. Soc.*, 2015, **137**, 4288–4291.

50 Y. Hori, H. Wakebe, T. Tsukamoto and O. Koga, *Electrochim. Acta*, 1994, **39**, 1833–1839.

51 Y. Hori, *Mod. Aspects Electrochem.*, 2008, **42**, 89–189.

52 Y. Hori, A. Murata and R. Takahashi, *J. Chem. Soc., Faraday Trans. 1*, 1989, **85**, 2309–2326.

53 Y. Hori, A. Murata, R. Takahashi and S. Suzuki, *J. Am. Chem. Soc.*, 1987, **109**, 5022–5023.

54 Y. Hori, A. Murata, R. Takahashi and S. Suzuki, *Chem. Lett.*, 1987, **16**, 1665–1668.

55 R. L. Cook, R. C. MacDuff and A. F. Sammells, *J. Electrochem. Soc.*, 1989, **136**, 1982.

56 Y. Hori, O. Koga, H. Yamazaki and T. Matsuo, *Electrochim. Acta*, 1995, **40**, 2617–2622.

57 N. Hoshi and Y. Hori, *Electrochim. Acta*, 2000, **45**, 4263–4270.

58 S. Sakaki, *J. Am. Chem. Soc.*, 1992, **114**, 2055–2062.

59 S. Taguchi and A. Aramata, *Electrochim. Acta*, 1994, **39**, 2533–2537.

60 A. Bagger, W. Ju, A. S. Varela, P. Strasser and J. Rossmeisl, *ChemPhysChem*, 2017, **18**, 3266–3273.

61 S. Sen, D. Liu and G. T. R. Palmore, *ACS Catal.*, 2014, **4**, 3091–3095.

62 C. W. Li and M. W. Kanan, *J. Am. Chem. Soc.*, 2012, **134**, 7231–7234.

63 W. J. Luo, X. W. Nie, M. J. Janik and A. Asthagiri, *ACS Catal.*, 2016, **6**, 219–229.

64 F. Calle-Vallejo and M. T. M. Koper, *Angew. Chem., Int. Ed.*, 2013, **52**, 7282–7285.

65 A. A. Peterson and J. K. Nørskov, *J. Phys. Chem. Lett.*, 2012, **3**, 251–258.

66 F. Abild-Pedersen, J. Greeley, F. Studt, J. Rossmeisl, T. R. Munter, P. G. Moses, E. Skulason, T. Bligaard and J. K. Norskov, *Phys. Rev. Lett.*, 2007, **99**, 016105.

67 J. Greeley, *Annu. Rev. Chem. Biomol. Eng.*, 2016, **7**, 605–635.

68 P. Hirunsit, W. Soodsawang and J. Limtrakul, *J. Phys. Chem. C*, 2015, **119**, 8238–8249.

69 F. L. Jia, X. X. Yu and L. Z. Zhang, *J. Power Sources*, 2014, **252**, 85–89.

70 X. Guo, Y. X. Zhang, C. Deng, X. Y. Li, Y. F. Xue, Y. M. Yan and K. Sun, *Chem. Commun.*, 2015, **51**, 1345–1348.

71 S. Rasul, D. H. Anjum, A. Jedidi, Y. Minenkov, L. Cavallo and K. Takanabe, *Angew. Chem., Int. Ed.*, 2015, **54**, 2146–2150.

72 L. Lu, X. F. Sun, J. Ma, D. X. Yang, H. H. Wu, B. X. Zhang, J. L. Zhang and B. X. Han, *Angew. Chem.*, 2018, **130**, 14345–14349.

73 M. L. Zhang, Z. D. Zhang, Z. H. Zhao, H. Huang, D. H. Anjum, D. S. Wang, J. H. He and K. W. Huang, *ACS Catal.*, 2021, **11**, 11103–11108.

74 S. Sarfraz, A. T. Garcia-Esparza, A. Jedidi, L. Cavallo and K. Takanabe, *ACS Catal.*, 2016, **6**, 2842–2851.

75 M. Li, J. J. Wang, P. Li, K. Chang, C. L. Li, T. Wang, B. Jiang, H. B. Zhang, H. M. Liu, Y. Yamauchi, N. Umezawa and J. H. Ye, *J. Mater. Chem. A*, 2016, **4**, 4776–4782.

76 M. X. Chen, S. P. Wan, L. X. Zhong, D. B. Liu, H. B. Yang, C. C. Li, Z. Q. Huang, C. T. Liu, J. Chen, H. G. Pan, D. S. Li, S. Z. Li, Q. Y. Yan and B. Liu, *Angew. Chem., Int. Ed.*, 2021, **60**, 26233–26237.

77 R. Zhou, X. Fan, X. X. Ke, J. Xu, X. Zhao, L. Jia, B. B. Pan, N. Han, L. X. Li, X. J. Liu, J. Luo, H. P. Lin and Y. G. Li, *Nano Lett.*, 2021, **21**, 4092–4098.

78 J. Monzó, Y. Malewski, R. Kortlever, F. J. Vidal-Iglesias, J. Solla-Gullón, M. T. M. Koper and P. Rodriguez, *J. Mater. Chem. A*, 2015, **3**, 23690–23698.

79 E. L. Clark, C. Hahn, T. F. Jaramillo and A. T. Bell, *J. Am. Chem. Soc.*, 2017, **139**, 15848–15857.

80 D. Ren, B. S. H. Ang and B. S. Yeo, *ACS Catal.*, 2016, **6**, 8239–8247.

81 Z. N. Wei, W. W. Wang, T. Shao, S. B. Yang, C. Liu, D. H. Si, R. Cao and M. N. Cao, *Angew. Chem.*, 2024, **64**, e202417066.

82 J. Christophe, T. Doneux and C. Buess-Herman, *Electrocatalysis*, 2012, **3**, 139–146.

83 T. Kottakkat, K. Klingan, S. Jiang, Z. P. Jovanov, V. H. Davies, G. A. M. El-Nagar, H. Dau and C. Roth, *ACS Appl. Mater. Interfaces*, 2019, **11**, 14734–14744.

84 Z. Y. Chang, S. J. Huo, W. Zhang, J. H. Fang and H. L. Wang, *J. Phys. Chem. C*, 2017, **121**, 11368–11379.

85 H. S. Jeon, J. Timoshenko, F. Scholten, I. Sinev, A. Herzog, F. T. Haase and B. R. Cuenya, *J. Am. Chem. Soc.*, 2019, **141**, 19879–19887.

86 L. Wang, H. J. Peng, S. Lamaison, Z. F. Qi, D. M. Koshy, M. B. Stevens, D. Wakerley, J. A. Zamora Zeledón, L. A. King, L. Zhou, Y. C. Lai, M. Fontecave, J. Gregoire, F. Abild-Pedersen, T. F. Jaramillo and C. Hahn, *Chem. Catal.*, 2021, **1**, 663–680.

87 D. Kim, J. Resasco, Y. Yu, A. M. Asiri and P. D. Yang, *Nat. Commun.*, 2014, **5**, 4948.

88 C. Choi, J. Cai, C. Lee, H. M. Lee, M. J. Xu and Y. Huang, *Nano Res.*, 2021, **14**, 3497–3501.

89 Y. J. Tak, J. A. Kwon, D. Y. Shin, A. Soon and D. H. Lim, *Surf. Interfaces*, 2022, **31**, 102030.

90 X. L. Wang, J. F. de Araújo, W. Ju, A. Bagger, H. Schmies, S. Kühl, J. Rossmeisl and P. Strasser, *Nat. Nanotechnol.*, 2019, **14**, 1063–1070.

91 T. Möller, W. Ju, A. Bagger, X. L. Wang, F. Luo, T. N. Thanh, A. S. Varela, J. Rossmeisl and P. Strasser, *Energy Environ. Sci.*, 2019, **12**, 640–647.

92 S. Y. Liang, L. Huang, Y. S. Gao, Q. Wang and B. Liu, *Adv. Sci.*, 2021, **8**, 2102886.

93 S. Lu, Y. Zhang, M. F. Mady, O. E. Eleri, W. M. Tucho, M. Mazur, A. Li, F. L. Lou, M. Gu and Z. X. Yu, *ChemSusChem*, 2022, **15**, e202200870.

94 J. L. Wang, Y. C. Huang, Y. Q. Wang, H. Deng, Y. C. Shi, D. X. Wei, M. T. Li, C. L. Dong, H. Jin, S. S. Mao and S. H. Shen, *ACS Catal.*, 2023, **13**, 2374–2385.

95 C. B. Chen, Y. F. Li, S. Yu, S. Louisia, J. B. Jin, M. F. Li, M. B. Ross and P. D. Yang, *Joule*, 2020, **4**, 1688–1699.

96 B. Cao, F. Z. Li and J. Gu, *ACS Catal.*, 2022, **12**, 9735–9752.

97 Y. Liu, H. M. Chen, Y. Yang, C. Jiao, W. K. Zhu, Y. P. Zhang, X. J. Wu, J. J. Mao and Z. W. Zhuo, *Energy Environ. Sci.*, 2023, **16**, 5185–5195.

98 R. Yang, J. Y. Duan, P. P. Dong, Q. L. Wen, M. Wu, Y. W. Liu, Y. Liu, H. Q. Li and T. Y. Zhai, *Angew. Chem., Int. Ed.*, 2022, **61**, e202116706.

99 B. Zhang, L. L. Wang, D. Li, Z. M. Li, R. Bu and Y. Y. Lu, *Chem. Catal.*, 2022, **2**, 3395–3429.

100 D. X. Wei, Y. Q. Wang, C. L. Dong, Z. Q. Zhang, X. Y. Wang, Y. C. Huang, Y. C. Shi, X. L. Zhao, J. L. Wang, R. Long, Y. J. Xiong, F. Dong, M. T. Li and S. H. Shen, *Angew. Chem., Int. Ed.*, 2023, **62**, e202217369.

101 T. Y. Zhang, Z. Y. Li, J. F. Zhang and J. J. Wu, *J. Catal.*, 2020, **387**, 163–169.

102 D. Niu, C. Wei, Z. Lu, Y. Y. Fang, B. Liu, D. Sun, X. B. Hao, H. G. Pan and G. M. Wang, *Molecules*, 2021, **26**, 2175.

103 S. Dongare, N. Singh and H. Bhunia, *Appl. Surf. Sci.*, 2021, **556**, 149790.

104 T. Luo, K. Liu, J. W. Fu, S. Y. Chen, H. M. Li, J. H. Hu and M. Liu, *J. Energy Chem.*, 2022, **70**, 219–223.

105 S. S. Zhang, S. L. Zhao, D. X. Qu, X. J. Liu, Y. P. Wu, Y. H. Chen and W. Huang, *Small*, 2021, **17**, 2102293.

106 N. Ling, J. G. Zhang, M. Wang, Z. Wang, Z. Y. Mi, S. B. Dolmanan, M. S. Zhang, B. Q. Wang, W. R. Leow, J. Zhang and Y. W. Lum, *Angew. Chem., Int. Ed.*, 2023, **62**, e202308782.

107 M. L. Frisch, L. F. Wu, C. Atlan, Z. Ren, M. Han, R. Tucoulou, L. Liang, J. S. Lu, A. Guo, H. N. Nong, A. Arinchtein, M. Sprung, J. Villanova, M. I. Richard and P. Strasser, *Nat. Commun.*, 2023, **14**, 7833.

108 T. Y. Zhang, J. C. Bui, Z. Y. Li, A. T. Bell, A. Z. Weber and J. J. Wu, *Nat. Catal.*, 2022, **5**, 202–211.

109 M. Liu, Q. Y. Wang, T. Luo, M. Herran, X. Y. Cao, W. R. Liao, L. Zhu, H. M. Li, A. Stefancu, Y. R. Lu, T. S. Chan, E. Pensa, C. Ma, S. G. Zhang, R. Y. Xiao and E. Cortes, *J. Am. Chem. Soc.*, 2024, **146**, 468–475.

110 M. Jouny, G. S. Hutchings and F. Jiao, *Nat. Catal.*, 2019, **2**, 1062–1070.

111 G. L. Wu, Y. R. Song, Q. Zheng, C. Long, T. Fan, Z. J. Yang, X. W. Huang, Q. Li, Y. L. Sun, L. L. Zuo, S. B. Lei and Z. Y. Tang, *Adv. Energy Mater.*, 2022, **12**, 2202054.

112 Y. Xie, P. F. Ou, X. Wang, Z. Y. Xu, Y. C. Li, Z. Y. Wang, J. E. Huang, J. Wicks, C. McCallum, N. Wang, Y. H. Wang, T. X. Chen, B. T. W. Lo, D. Sinton, J. C. Yu, Y. Wang and E. H. Sargent, *Nat. Catal.*, 2022, **5**, 564–570.

113 Y. J. Chen, X. Y. Li, Z. Chen, A. Ozden, J. E. Huang, P. F. Ou, J. C. Dong, J. Q. Zhang, C. Tian, B. H. Lee, X. Y. Wang, S. J. Liu, Q. Y. Qu, S. S. Wang, Y. Xu, R. K. Miao, Y. Zhao, Y. J. Liu, C. Y. Qiu, J. Abed, H. Z. Liu, H. Shin, D. S. Wang, Y. D. Li, D. Sinton and E. H. Sargent, *Nat. Nanotechnol.*, 2024, **19**, 311–318.

114 C. T. Dinh, T. Burdyny, M. G. Kibria, A. Seifitokaldani, C. M. Gabardo, F. P. G. de Arquer, A. Kiani, J. P. Edwards, P. D. Luna, O. S. Bushuyev, C. Q. Zou, R. Q. Bermudez, Y. J. Pang, D. Sinton and E. H. Sargent, *Science*, 2018, **360**, 783–787.

115 J. Li, X. X. Chang, H. C. Zhang, A. S. Malkani, M. J. Cheng, B. J. Xu and Q. Lu, *Nat. Commun.*, 2021, **12**, 3264.

116 S. J. Mu, H. L. Lu, Q. B. Wu, L. Li, R. J. Zhao, C. Long and C. H. Cui, *Nat. Commun.*, 2022, **13**, 3694.

117 J. Gao, H. Zhang, X. Y. Guo, J. S. Luo, S. M. Zakeeruddin, D. Ren and M. Grätzel, *J. Am. Chem. Soc.*, 2019, **141**, 18704–18714.

118 Y. C. Li, Z. Y. Wang, T. G. Yuan, D. H. Nam, M. C. Luo, J. Wicks, B. Chen, J. Li, F. W. Li, F. P. G. de Arquer,

Y. Wang, C. T. Dinh, O. Voznyy, D. Sinton and E. H. Sargent, *J. Am. Chem. Soc.*, 2019, **141**, 8584–8591.

119 L. R. L. Ting, O. Piqué, S. Y. Lim, M. Tanhaei, F. Calle-Vallejo and B. S. Yeo, *ACS Catal.*, 2020, **10**, 4059–4069.

120 C. Y. Zhu, L. H. Zhou, Z. B. Zhang, C. L. Yang, G. S. Shi, S. W. Zhao, H. L. Gu, J. Wu, X. Y. Gao, Y. F. Li, K. H. Liu, S. Dai and L. M. Zhang, *Chem*, 2022, **8**, 3288–3301.

121 H. S. Feng, C. Y. Chen, S. Wang, M. Zhang, H. Ding, Y. J. Liang and X. Zhang, *J. Phys. Chem. Lett.*, 2022, **13**, 8002–8009.

122 S. Y. Kuang, Y. Q. Su, M. L. Li, H. Liu, H. Y. Chuai, X. Y. Chen, E. J. M. Hensen, T. J. Meyer, S. Zhang and X. B. Ma, *Proc. Natl. Acad. Sci. U. S. A.*, 2023, **120**, e2214175120.

123 P. Iyengar, M. J. Kolb, J. R. Pankhurst, F. C. Vallejo and R. Buonsanti, *ACS Catal.*, 2021, **11**, 4456–4463.

124 H. Cao, Z. S. Zhang, J. W. Chen and Y. G. Wang, *ACS Catal.*, 2022, **12**, 6606–6617.

125 W. D. Dai, K. W. Wan, K. L. Pang, J. Guo, S. Y. Liu, K. Y. Wu, C. Y. Tang, Y. J. Sun, X. H. Shi, Z. Y. Tang, C. Long and F. Dong, *Chem*, 2025, **11**, 102345.

126 J. F. Huang, M. Mensi, E. Oveisi, V. Mantella and R. Buonsanti, *J. Am. Chem. Soc.*, 2019, **141**, 2490–2499.

127 W. B. Zhang, Y. Yang, Y. Tang and Q. S. Gao, *J. Energy Chem.*, 2022, **70**, 414–436.

128 C. Y. Zhu, S. W. Zhao, G. S. Shi and L. M. Zhang, *ChemSusChem*, 2022, **15**, e202200068.

129 C. Long, K. W. Wan, Y. Chen, L. Li, Y. H. Jiang, C. Y. Yang, Q. B. Wu, G. L. Wu, P. Xu, J. Li, X. H. Shi, Z. Y. Tang and C. H. Cui, *J. Am. Chem. Soc.*, 2024, **146**, 16039–16051.

130 C. Long, X. L. Liu, K. W. Wan, Y. H. Jiang, P. F. An, C. Y. Yang, G. L. Wu, W. Y. Wang, J. Guo, L. Li, K. L. Pang, Q. Li, C. H. Cui, S. Q. Liu, T. Tan and Z. Y. Tang, *Sci. Adv.*, 2023, **9**, eadi6119.

131 W. J. Xu, H. S. Shang, J. Guan, X. Y. Yang, X. Y. Jin, L. M. Tao and Z. Q. Shao, *Adv. Funct. Mater.*, 2025, **35**, 2412812.

132 W. Z. Zheng, X. X. Yang, Z. J. Li, B. Yang, Q. H. Zhang, L. C. Lei and Y. Hou, *Angew. Chem.*, 2023, **135**, e202307283.

133 P. P. Yang and M. R. Gao, *Chem. Soc. Rev.*, 2023, **52**, 4343–4380.

134 X. Y. Tan, C. Yu, Y. W. Ren, S. Cui, W. B. Li and J. S. Qiu, *Energy Environ. Sci.*, 2021, **14**, 765–780.